Nano Hexapod - Optimal Geometry

Dehaeze Thomas

April 1, 2025

Contents

- In the conceptual design phase, the geometry of the Stewart platform was chosen arbitrarily and not optimized
- In the detail design phase, we want to see if the geometry can be optimized to improve the overall performances
- Optimization criteria: mobility, stiffness, decoupling between the struts for decentralized control, dynamical decoupling in the cartesian frame

Outline:

- Review of Stewart platform (Section 1) Geometry, Actuators, Sensors, Joints
- Effect of geometry on the Stewart platform characteristics (Section 2)
- Cubic configuration: special architecture that received many attention in the literature. We want to see the special properties of this architecture and if this can be applied for the nano hexapod (Section 3)
- Presentation of the obtained geometry for the nano hexapod (Section 4)

1 Review of Stewart platforms

- As was explained in the conceptual phase, Stewart platform have the following key elements:
  - Two plates connected by six struts
  - Each strut is composed of:
    - a flexible joint at each end
    - an actuator
    - one or several sensors
- The exact geometry (i.e. position of joints and orientation of the struts) can be chosen freely depending on the application.
- This results in many different designs found in the literature.
- The focus is here made on Stewart platforms for nano-positioning and vibration control. Long stroke stewart platforms are not considered here as their design impose other challenges. Some Stewart platforms found in the literature are listed in Table 1.1
- All presented Stewart platforms are using flexible joints, as it is a prerequisites for nano-positioning capabilities.
- Most of stewart platforms are using voice coil actuators or piezoelectric actuators. The actuators used for the Stewart platform will be chosen in the next section.
- Depending on the application, various sensors are integrated in the struts or on the plates such as force sensors, inertial sensors or relative displacement sensors. The choice of sensor for the nano-hexapod will be described in the next section.
- Flexible joints can also have various implementations. This will be discussed in the next section.
- There are two main categories of Stewart platform geometry:
  - Cubic architecture (Figure 1.1). Struts are positioned along 6 sides of a cubic (and are therefore orthogonal to each other). Such specific architecture has some special properties that will be studied in Section 3.
  - Non-cubic architecture (Figure 1.2) The orientation of the struts and position of the joints are chosen based on performances criteria. Some of which are presented in Section 2

Conclusion:

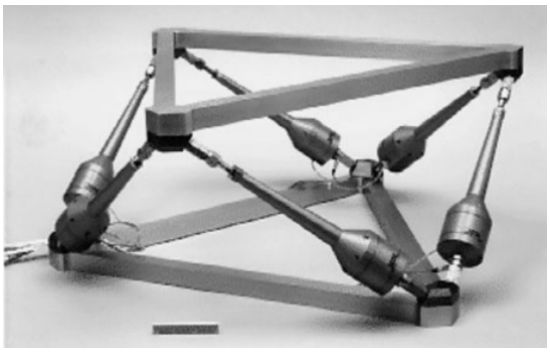

(a) California Institute of Technology - USA

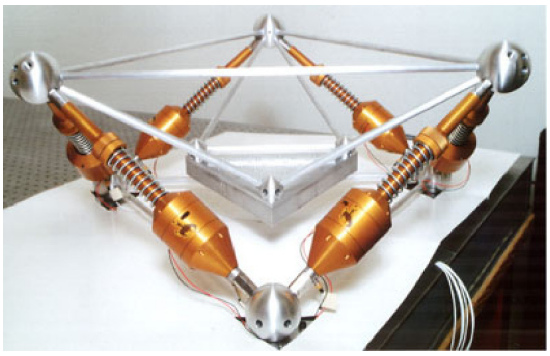

(b) University of Wyoming - USA

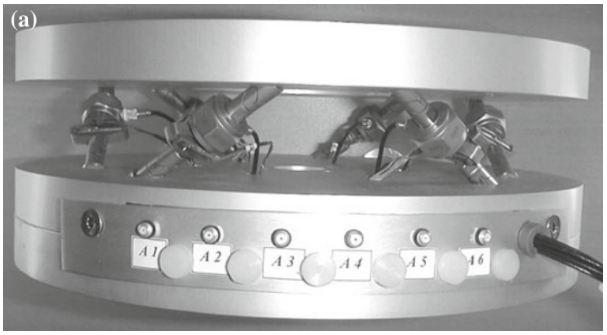

(c) ULB - Belgium

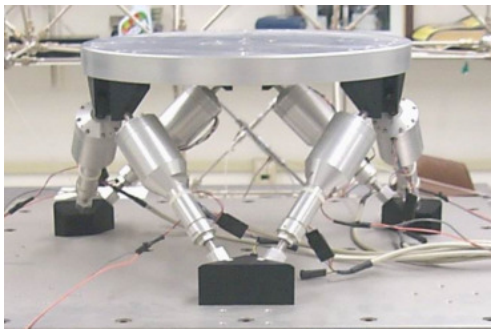

(d) Naval Postgraduate School - USA

Figure 1.1: Some examples of developped Stewart platform with Cubic geometry. (a), (b), (c), (d)

Table 1.1: Examples of Stewart platform developed. When not specifically indicated, sensors are included in the struts. All presented Stewart platforms are using flexible joints. The table is ordered by appearance in the literature

	Geometry	Actuators	Sensors	Reference
	Cubic	Magnetostrictive	Force, Accelerometers	[1]–[3]
Figure 1.1a	Cubic	Voice Coil (0.5 mm)	Force	[4], [5]
	Cubic	Voice Coil (10 mm)	Force, LVDT, Geophones	[6]–[8]
Figure 1.1b	Cubic	Voice Coil	Force	[9]–[13]
	Cubic	Piezoelectric (25 μm)	Force	[14]
Figure 1.1c	Cubic	APA (50 μm)	Force	[15]
Figure 1.2a	Non-Cubic	Voice Coil	Accelerometers	[16]
	Cubic	Voice Coil	Force	[17], [18]
Figure 1.1d	Cubic	Piezoelectric (50 μm)	Geophone	[19]
	Non-Cubic	Piezoelectric (16 μm)	Eddy Current	[20]
	Cubic	Piezoelectric (120 μm)	(External) Capacitive	[21], [22]
	Non-Cubic	Piezoelectric (160 μm)	(External) Capacitive	[23]
Figure 1.2b	Non-cubic	Magnetostrictive	Accelerometer	[24]
	Non-Cubic	Piezoelectric	Strain Gauge	[25]
	Cubic	Voice Coil	Accelerometer	[26]–[28]
	Cubic	Piezoelectric	Force	[29]
	Almost cubic	Voice Coil	Force, Accelerometer	[30], [31]
Figure 1.2c	Almost cubic	Piezoelectric	Force, Strain gauge	[32]
Figure 1.2d	Non-Cubic	3-phase rotary motor	Rotary Encoder	[33], [34]

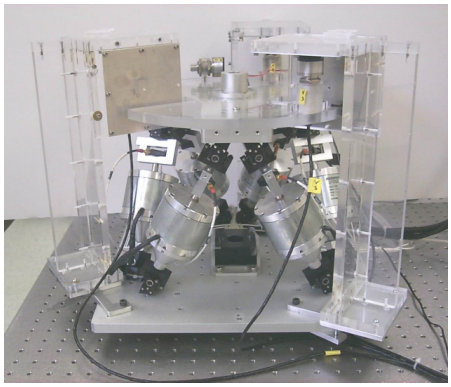

(a) Naval Postgraduate School - USA

(b) Beihang University - China

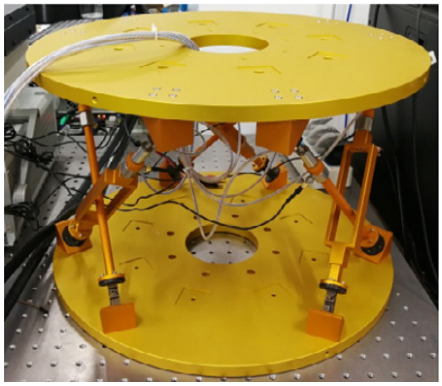

(c) Nanjing University - China

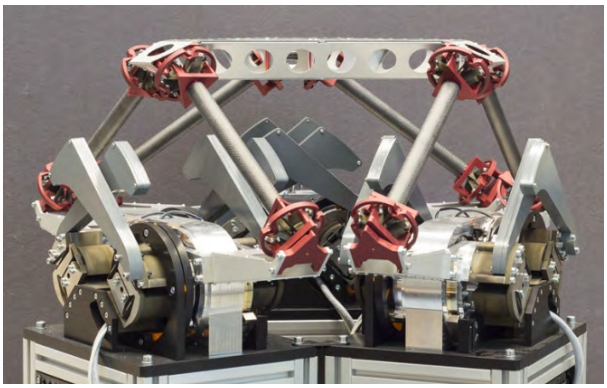

(d) University of Twente - Netherlands

Figure 1.2: Some examples of developped Stewart platform with non-cubic geometry. (a), (b), (c), (d)

- Various Stewart platform designs:
  - geometry, sizes, orientation of struts
  - Lot's have a "cubic" architecture that will be discussed in Section 3
  - actuator types
  - various sensors
  - flexible joints
- The effect of geometry on the properties of the Stewart platform is studied in section 2
- It is determined what is the optimal geometry for the NASS

2 Effect of geometry on Stewart platform properties

- As was shown during the conceptual phase, the geometry of the Stewart platform influences:
  - the stiffness and compliance properties
  - the mobility or workspace
  - the force authority
  - the dynamics of the manipulator
- It is therefore important to understand how the geometry impact these properties, and to be able to optimize the geometry for a specific application.

One important tool to study this is the Jacobian matrix which depends on the $\boldsymbol{b}_i$ (join position w.r.t top platform) and $\hat{\boldsymbol{s}}_i$ (orientation of struts). The choice of frames ($\{A\}$ and $\{B\}$), independently of the physical Stewart platform geometry, impacts the obtained kinematics and stiffness matrix, as it is defined for forces and motion evaluated at the chosen frame.

2.1 Platform Mobility / Workspace

The mobility of the Stewart platform (or any manipulator) is here defined as the range of motion that it can perform. It corresponds to the set of possible pose (i.e. combined translation and rotation) of frame {B} with respect to frame {A}. It is therefore a six dimensional property which is difficult to represent. Depending on the applications, only the translation mobility (i.e. fixed orientation workspace) or the rotation mobility may be represented. This is equivalent as to project the six dimensional value into a 3 dimensional space, easier to represent.

Mobility of parallel manipulators are inherently difficult to study as the translational and orientation workspace are coupled **merlet02˙still**. Things are getting much more simpler when considering small motions as the Jacobian matrix can be considered constant and the equations are linear.

As was shown during the conceptual phase, for small displacements, the Jacobian matrix can be used

to link the strut motion to the motion of frame B with respect to A through equation (2.1).

$$\begin{bmatrix} \delta l_1 \\ \delta l_2 \\ \delta l_3 \\ \delta l_4 \\ \delta l_5 \\ \delta l_6 \end{bmatrix} = \begin{bmatrix} {}^A\hat{\boldsymbol{s}}_1{}^T & ({}^A\boldsymbol{b}_1 \times {}^A\hat{\boldsymbol{s}}_1)^T \\ {}^A\hat{\boldsymbol{s}}_2{}^T & ({}^A\boldsymbol{b}_2 \times {}^A\hat{\boldsymbol{s}}_2)^T \\ {}^A\hat{\boldsymbol{s}}_3{}^T & ({}^A\boldsymbol{b}_3 \times {}^A\hat{\boldsymbol{s}}_3)^T \\ {}^A\hat{\boldsymbol{s}}_4{}^T & ({}^A\boldsymbol{b}_4 \times {}^A\hat{\boldsymbol{s}}_4)^T \\ {}^A\hat{\boldsymbol{s}}_5{}^T & ({}^A\boldsymbol{b}_5 \times {}^A\hat{\boldsymbol{s}}_5)^T \\ {}^A\hat{\boldsymbol{s}}_6{}^T & ({}^A\boldsymbol{b}_6 \times {}^A\hat{\boldsymbol{s}}_6)^T \end{bmatrix} \begin{bmatrix} \delta x \\ \delta y \\ \delta z \\ \delta\theta_x \\ \delta\theta_y \\ \delta\theta_z \end{bmatrix} \tag{2.1}$$

Therefore, the mobility of the Stewart platform (set of $[\delta x\ \delta y\ \delta z\ \delta\theta_x\ \delta\theta_y\ \delta\theta_z]$) depends on:

- the stroke of each strut
- the geometry of the Stewart platform (embodied in the Jacobian matrix)

More specifically:

- the XYZ mobility only depends on the si (orientation of struts)
- the mobility in rotation depends on bi (position of top joints)

Mobility in translation Here, for simplicity, only translations are first considered (i.e. fixed orientation of the Stewart platform):

- Let's consider a general Stewart platform geometry shown in Figure 2.1a.
- In the general case: the translational mobility can be represented by a 3D shape with 12 faces (each actuator limits the stroke along its orientation in positive and negative directions). The faces are therefore perpendicular to the strut direction. The obtained mobility for the considered stewart platform geometry is shown in Figure 2.1b. In reality, the workspace boundaries are portion of spheres, but they are well approximated by flat surfaces for short stroke hexapods
- Considering an actuator stroke of $\pm d$, the mobile platform can be translated in any direction with a stroke of d This means that a sphere with radius d is contained in the general shape as illustrated in Figure 2.1b. The sphere will touch the shape along six lines defined by the strut axes.

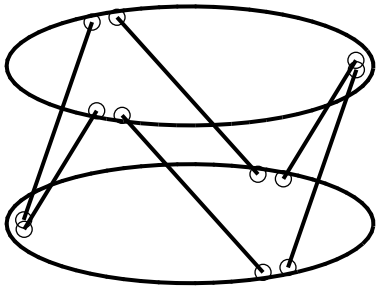

(a) Stewart platform geometry

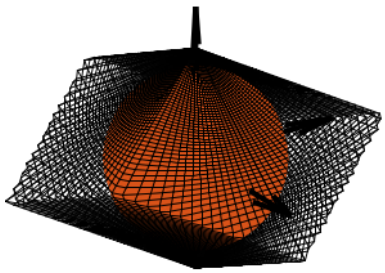

(b) Translational mobility

Figure 2.1: Example of one Stewart platform (a) and associated translational mobility (b)

To better understand how the geometry of the Stewart platform impacts the translational mobility, two configurations are compared:

- Struts oriented horizontally (Figure 2.2a). This leads to having more stroke in the horizontal direction and less stroke in the vertical direction (Figure 2.2c).
- Struts oriented vertically (Figure 2.2b). More stroke in vertical direction

It can be counter intuitive to have less stroke in the direction of the struts. This is because the struts are forming a lever mechanism that amplifies the motion. The amplification factor increases when the struts have an high angle with the direction and motion and is equal to one when it is aligned with the direction of motion.

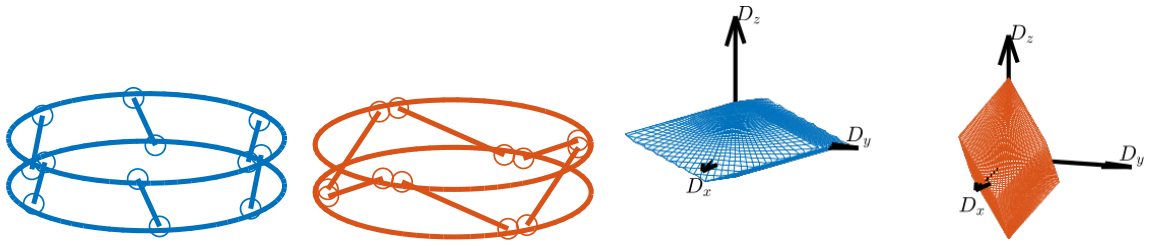

(a) Vertical struts **(b)** Horizontal struts **(c)** Translational mobility

Figure 2.2: Effect of strut orientation on the obtained mobility in translation. Two Stewart platform geometry are considered: struts oriented vertically (a) and struts oriented vertically (b). Obtained mobility for both geometry are shown in (c).

Mobility in rotation As shown by equation (2.1), the rotational mobility depends both on the orientation of the struts and on the location of the top joints.

Similarly to the translational case, to increase the rotational mobility in one direction, it is advantageous to have the struts more perpendicular to the rotational direction.

For instance, having the struts more vertical (Figure 2.2a) gives less rotational stroke along the vertical direction than having the struts oriented more horizontally (Figure 2.2b).

Two cases are considered with same strut orientation but with different top joints positions:

- struts close to each other (Figure 2.3a)
- struts further apart (Figure 2.3b)

The mobility for pure rotations are compared in Figure 2.3c. Note that the same strut stroke are considered in both cases to evaluate the mobility. Having struts further apart decreases the "level arm" and therefore the rotational mobility is reduced.

For rotations and translations, having more mobility also means increasing the effect of actuator noise on the considering degree of freedom. Somehow, the level arm is increased, so any strut vibration gets amplified. Therefore, the designed Stewart platform should just have the necessary mobility.

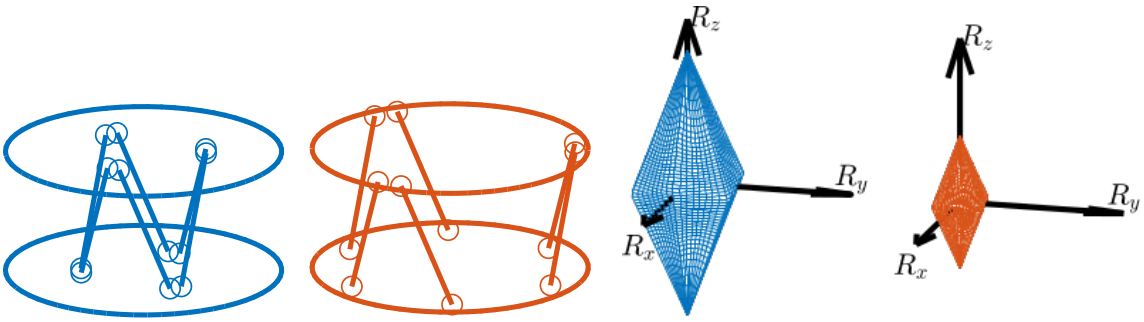

(a) Struts close together **(b)** Struts far apart **(c)** Rotational mobility

Figure 2.3: Effect of strut position on the obtained mobility in rotation. Two Stewart platform geometry are considered: struts close to each other (a) and struts further appart (b). Obtained mobility for both geometry are shown in (c).

Combined translations and rotations It is possible to consider combined translations and rotations. Displaying such mobility is more complex. It will be used for the nano-hexapod to verify that the obtained design has the necessary mobility.

For a fixed geometry and a wanted mobility (combined translations and rotations), it is possible to estimate the required minimum actuator stroke. It will be done in Section 4 to estimate the required actuator stroke for the nano-hexapod geometry.

2.2 Stiffness

Stiffness matrix:

- defines how the nano-hexapod deforms (frame $\{B\}$ with respect to frame $\{A\}$) due to static forces/torques applied on $\{B\}$.
- It depends on the Jacobian matrix (i.e. the geometry) and the strut axial stiffness (2.2)
- The contribution of joints stiffness is here not considered **mcinroy02˙model˙desig˙flexur˙joint˙stewar**, [11]

$$\boldsymbol{K} = \boldsymbol{J}^T \boldsymbol{\mathcal{K}} \boldsymbol{J} \tag{2.2}$$

It is assumed that the stiffness of all strut is the same: $\boldsymbol{\mathcal{K}} = k \cdot \mathbf{I}_6$. Obtained stiffness matrix linearly depends on the strut stiffness k, and is structured as shown in (2.3).

$$\boldsymbol{K} = k\boldsymbol{J}^T\boldsymbol{J} = k \left[\begin{array}{c|c} \Sigma_{i=0}^{6} \hat{\boldsymbol{s}}_i \cdot \hat{\boldsymbol{s}}_i^T & \Sigma_{i=0}^{6} \hat{\boldsymbol{s}}_i \cdot ({}^A\boldsymbol{b}_i \times {}^A\hat{\boldsymbol{s}}_i)^T \\ \hline \Sigma_{i=0}^{6} ({}^A\boldsymbol{b}_i \times {}^A\hat{\boldsymbol{s}}_i) \cdot \hat{\boldsymbol{s}}_i^T & \Sigma_{i=0}^{6} ({}^A\boldsymbol{b}_i \times {}^A\hat{\boldsymbol{s}}_i) \cdot ({}^A\boldsymbol{b}_i \times {}^A\hat{\boldsymbol{s}}_i)^T \end{array} \right] \tag{2.3}$$

Translation Stiffness As shown by (2.3), the translation stiffnesses (the 3x3 top left terms of the stiffness matrix):

- Only depends on the orientation of the struts and not their location: $\hat{\boldsymbol{s}}_i \cdot \hat{\boldsymbol{s}}_i^T$
- Extreme case: all struts are vertical $s_i = [0,\ 0,\ 1]$ =¿ vertical stiffness of $6k$, but null stiffness in X and Y directions
- If two struts along X, two struts along Y, and two struts along Z =¿ $\hat{\boldsymbol{s}}_i \cdot \hat{\boldsymbol{s}}_i^T = 2\boldsymbol{I}_3$ Stiffness is well distributed along directions. This corresponds to the cubic architecture presented in Section 3.

If struts more vertical (Figure 2.2a):

- increase vertical stiffness
- decrease horizontal stiffness
- increase Rx,Ry stiffness
- decrease Rz stiffness

Opposite conclusions if struts are not horizontal (Figure 2.2b).

Rotational Stiffness The rotational stiffnesses depends both on the orientation of the struts and on the location of the top joints (with respect to the considered center of rotation, i.e. the location of frame B).

Same orientation but increased distances (bi) by a factor 2 =¿ rotational stiffness increased by factor 4. Compact stewart platform of Figure 2.3a as therefore less rotational stiffness than the Stewart platform of Figure 2.3b.

Diagonal Stiffness Matrix Having the stiffness matrix $\boldsymbol{K}$ diagonal can be beneficial for control purposes as it would make the plant in the cartesian frame decoupled at low frequency. This depends on the geometry and on the chosen {B} frame. For specific geometry and chose of B frame, it is possible to have a diagonal K matrix.

This will be discussed in Section 3.1.

2.3 Dynamical properties

In the Cartesian Frame Dynamical equations (both in the cartesian frame and in the frame of the struts) for the Stewart platform were derived during the conceptual phase with simplifying assumptions (massless struts and perfect joints). The dynamics depends both on the geometry (Jacobian matrix) but also on the payload being placed on top of the platform.

Under very specific conditions, the equations of motion in the Cartesian frame (2.4) can be decoupled. These are studied in Section 3.2.

$$\frac{\mathcal{X}}{\mathcal{F}}(s) = (\boldsymbol{M}s^2 + \boldsymbol{J}^T\boldsymbol{\mathcal{C}}\boldsymbol{J}s + \boldsymbol{J}^T\boldsymbol{\mathcal{K}}\boldsymbol{J})^{-1} \tag{2.4}$$

In the frame of the Struts In the frame of the struts, the equations of motion (2.5) are well decoupled at low frequency. This is why most of Stewart platforms are controlled in the frame of the struts: bellow the resonance frequency, the system is decoupled and SISO control may be applied for each strut, independently of the payload being used.

$$\frac{\mathcal{L}}{\mathcal{f}}(s) = (\boldsymbol{J}^{-T}\boldsymbol{M}\boldsymbol{J}^{-1}s^2 + \boldsymbol{\mathcal{C}} + \boldsymbol{\mathcal{K}})^{-1} \tag{2.5}$$

Coupling between sensors (force sensors, relative position sensor, inertial sensors) in different struts may also be important for decentralized control. In section 3.3, it will be study if the Stewart platform geometry can be optimized to have lower coupling between the struts.

Conclusion

The effects of two changes in the manipulator's geometry, namely the position and orientation of the legs, are summarized in Table 2.1. These results could have been easily deduced based on some mechanical principles, but thanks to the kinematic analysis, they can be quantified.

These trade-offs give some guidelines when choosing the Stewart platform geometry.

Table 2.1: Effect of a change in geometry on the manipulator's stiffness, force authority and stroke

Struts	**Vertically Oriented**	**Increased separation**
Vertical stiffness	$\nearrow$	$=$
Horizontal stiffness	$\searrow$	$=$
Vertical rotation stiffness	$\searrow$	$\nearrow$
Horizontal rotation stiffness	$\nearrow$	$\nearrow$
Vertical stroke	$\searrow$	$=$
Horizontal stroke	$\nearrow$	$=$
Vertical rotation stroke	$\nearrow$	$\searrow$
Horizontal rotation stroke	$\searrow$	$\searrow$

3 The Cubic Architecture

The Cubic configuration for the Stewart platform was first proposed in [2]. This configuration is quite specific in the sense that the active struts are arranged in a mutually orthogonal configuration connecting the corners of a cube, as shown in Figure 3.1.

Typically, the struts have similar size than the cube's edge, as shown in Figure 3.1a. Practical implementations of such configuration are shown in Figures 1.1a, 1.1b and 1.1d.

It is also possible to have the struts length smaller than the cube's edge (Figure 3.1b). An example of such Stewart platform is shown in Figure 1.1c.

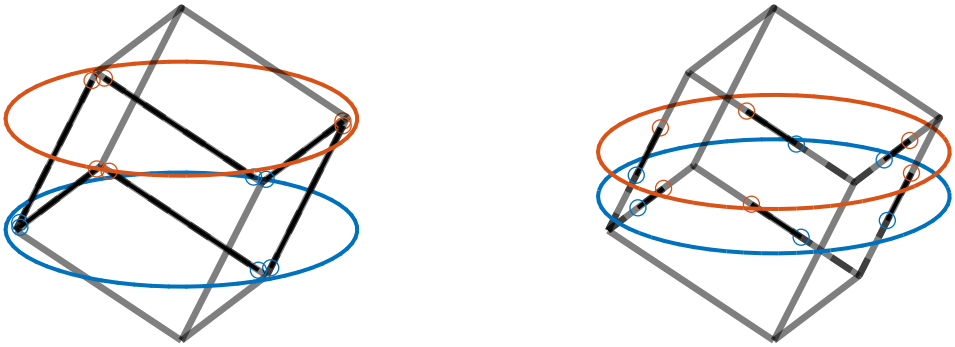

(a) sub caption a **(b)** sub caption b

Figure 3.1: Typical Stewart platform cubic architectures. (a) (b)

A number of properties are attributed to the cubic configuration, which have made this configuration widely popular ([2], [13], [18]):

- Simple kinematics relationships and dynamical analysis [2]
- Uniform stiffness in all directions [17]
- Uniform mobility **preumont18˙vibrat˙contr˙activ˙struc˙fourt˙edition**
- Minimization of the cross coupling between actuators and sensors in other struts [18]. This is attributed to the fact that the struts are orthogonal to each other. This is said to facilitate collocated sensor-actuator control system design, i.e. the implementation of decentralized control [2], [7].

Such properties are studied to see if they are useful for the nano-hexapod and the associated conditions:

- The mobility and stiffness properties of the cubic configuration are studied in Section 3.1.

- Dynamical decoupling is studied in Section 3.2
- Decentralized control, important for the NASS, is studied in Section 3.3

As the cubic architecture has some restrictions on the geometry, alternative designs are proposed in Section 3.4.

The goal is to determine if the cubic architecture is interesting for the nano-hexapod.

3.1 Static Properties

Stiffness matrix for the Cubic architecture Consider the cubic architecture shown in Figure 3.2a. The unit vectors corresponding to the edges of the cube are described by (3.1).

$$\hat{\boldsymbol{s}}_1 = \begin{bmatrix} \sqrt{2}/\sqrt{3} \\ 0 \\ 1/\sqrt{3} \end{bmatrix} \quad \hat{\boldsymbol{s}}_2 = \begin{bmatrix} -1/\sqrt{6} \\ -1/\sqrt{2} \\ 1/\sqrt{3} \end{bmatrix} \quad \hat{\boldsymbol{s}}_3 = \begin{bmatrix} -1/\sqrt{6} \\ 1/\sqrt{2} \\ 1/\sqrt{3} \end{bmatrix} \quad \hat{\boldsymbol{s}}_4 = \begin{bmatrix} \sqrt{2}/\sqrt{3} \\ 0 \\ 1/\sqrt{3} \end{bmatrix} \quad \hat{\boldsymbol{s}}_5 = \begin{bmatrix} -1/\sqrt{6} \\ -1/\sqrt{2} \\ 1/\sqrt{3} \end{bmatrix} \quad \hat{\boldsymbol{s}}_6 = \begin{bmatrix} -1/\sqrt{6} \\ 1/\sqrt{2} \\ 1/\sqrt{3} \end{bmatrix} \tag{3.1}$$

Coordinates of the cube's vertices relevant for the top joints, expressed with respect to the cube's center (3.2).

$$\tilde{\boldsymbol{b}}_1 = \tilde{\boldsymbol{b}}_2 = H_c \begin{bmatrix} \frac{1}{\sqrt{2}} \\ \frac{-\sqrt{3}}{\sqrt{2}} \\ \frac{1}{2} \end{bmatrix}, \quad \tilde{\boldsymbol{b}}_3 = \tilde{\boldsymbol{b}}_4 = H_c \begin{bmatrix} \frac{1}{\sqrt{2}} \\ \frac{\sqrt{3}}{\sqrt{2}} \\ \frac{1}{2} \end{bmatrix}, \quad \tilde{\boldsymbol{b}}_5 = \tilde{\boldsymbol{b}}_6 = H_c \begin{bmatrix} \frac{-2}{\sqrt{2}} \\ 0 \\ \frac{1}{2} \end{bmatrix} \tag{3.2}$$

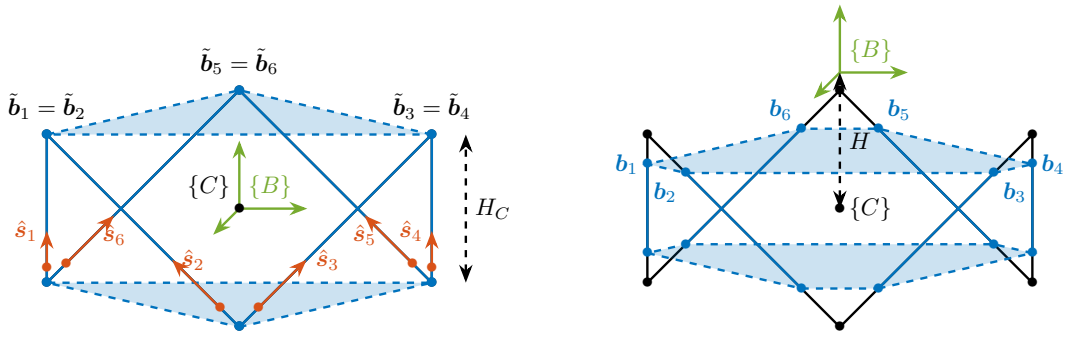

(a) Full cube **(b)** Cube's portion

Figure 3.2: Struts are represented un blue. The cube's center by a dot.

In that case (top joints at the cube's vertices), a diagonal stiffness matrix is obtained (3.3). Translation stiffness is twice the stiffness of the struts, and rotational stiffness is proportional to the square of the cube's size H_c.

$$\boldsymbol{K}_{\{B\}=\{C\}} = k \begin{bmatrix} 2 & 0 & 0 & 0 & 0 & 0 \\ 0 & 2 & 0 & 0 & 0 & 0 \\ 0 & 0 & 2 & 0 & 0 & 0 \\ 0 & 0 & 0 & \frac{3}{2}H_c^2 & 0 & 0 \\ 0 & 0 & 0 & 0 & \frac{3}{2}H_c^2 & 0 \\ 0 & 0 & 0 & 0 & 0 & 6H_c^2 \end{bmatrix} \tag{3.3}$$

But typically, the top joints are not placed at the cube's vertices but anywhere along the cube's edges (Figure 3.2b). In that case, the location of the top joints can be expressed by (3.4). But the computed stiffness matrix is the same (3.3).

$$\boldsymbol{b}_i = \tilde{\boldsymbol{b}}_i + \alpha \hat{\boldsymbol{s}}_i \tag{3.4}$$

The Stiffness matrix is therefore diagonal when the considered {B} frame is located at the center of the cube. for forces and torques applied on the top platform, but expressed at the center of the cube, and for translations and rotations of the top platform expressed with respect to the cube's center.

☐ Should I introduce the term "center of stiffness" here?

Effect of having frame $\{B\}$ off-centered However, as soon as the location of the A and B frames are shifted from the cube's center, off diagonal elements in the stiffness matrix appear.

Let's consider here a vertical shift as shown in Figure 3.2b. In that case, the stiffness matrix is (3.5). Off diagonal elements are increasing with the height difference between the cube's center and the considered B frame.

$$\boldsymbol{K}_{\{B\}\neq\{C\}} = k \begin{bmatrix} 2 & 0 & 0 & 0 & -2H & 0 \\ 0 & 2 & 0 & 2H & 0 & 0 \\ 0 & 0 & 2 & 0 & 0 & 0 \\ 0 & 2H & 0 & \frac{3}{2}H_c^2 + 2H^2 & 0 & 0 \\ -2H & 0 & 0 & 0 & \frac{3}{2}H_c^2 + 2H^2 & 0 \\ 0 & 0 & 0 & 0 & 0 & 6H_c^2 \end{bmatrix} \tag{3.5}$$

Such structure of the stiffness matrix is very typical with Stewart platform that have some symmetry, but not necessary only for cubic architectures.

Therefore, the stiffness of the cubic architecture is special only when considering a frame located at the center of the cube. This is not very convenient, as in the vast majority of cases, the interesting frame is located about the top platform.

Note that the cube's center needs not to be at the "center" of the Stewart platform. This can lead to interesting architectures shown in Section 3.4.

Uniform Mobility Uniform mobility in X,Y,Z directions (Figure 3.3a)

- This is somehow more uniform than other architecture

- A cube is obtained
- The length of the cube's edge is equal to the strut axial stroke
- Mobility in translation does not depend on the cube's size

Some have argue that the translational mobility of the Cubic Stewart platform is a sphere [11], and this is useful to be able to move equal amount in all directions. As shown here, this is wrong. It is possible the consider that the mobility is uniform along the directions of the struts, but usually these are not interesting directions.

Also show mobility in Rx,Ry,Rz (Figure 3.3b):

- more mobility in Rx and Ry than in Rz
- Mobility decreases with the size of the cube

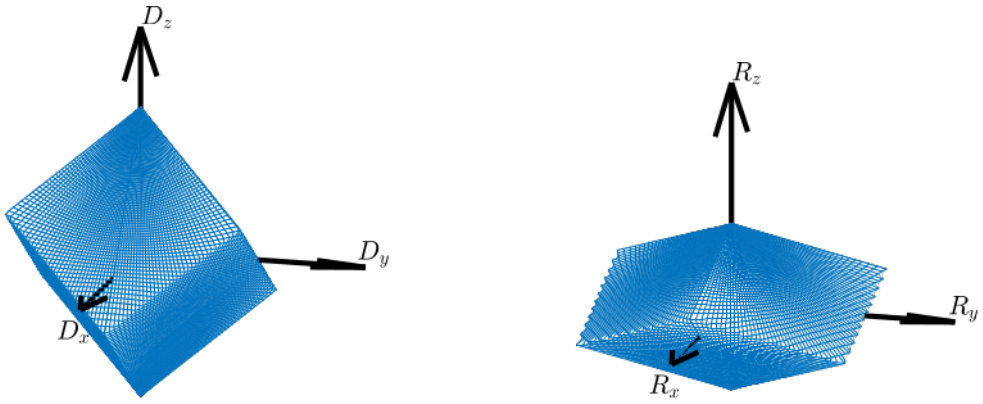

(a) Mobility in translation **(b)** Mobility in rotation

Figure 3.3: Mobility of a Stewart platform with Cubic architecture. Both for translations (a) and rotations (b)

3.2 Dynamical Decoupling

☐ [11] Why is this here?

In this section, the dynamics of the platform in the cartesian frame is studied. This corresponds to the transfer function from forces and torques $\mathcal{F}$ to translations and rotations $\mathcal{X}$ of the top platform. If relative motion sensor are located in each strut ($\mathcal{L}$ is measured), the pose $\mathcal{X}$ is computed using the Jacobian matrix as shown in Figure 3.4.

We want to see if the Stewart platform has some special properties for control in the cartesian frame.

Low frequency and High frequency coupling As was derived during the conceptual design phase, the dynamics from $\mathcal{F}$ to $\mathcal{X}$ is described by (3.6)

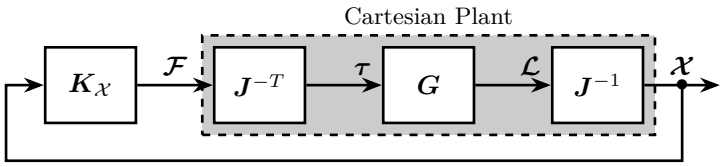

Figure 3.4: From Strut coordinate to Cartesian coordinate using the Jacobian matrix

$$\frac{\boldsymbol{\mathcal{X}}}{\boldsymbol{\mathcal{F}}}(s) = (\boldsymbol{M}s^2 + \boldsymbol{J}^T\boldsymbol{\mathcal{C}}\boldsymbol{J}s + \boldsymbol{J}^T\boldsymbol{\mathcal{K}}\boldsymbol{J})^{-1} \tag{3.6}$$

At low frequency: the static behavior of the platform depends on the stiffness matrix (3.7).

$$\frac{\boldsymbol{\mathcal{X}}}{\boldsymbol{\mathcal{F}}}(j\omega) \xrightarrow[\omega \to 0]{} \boldsymbol{K}^{-1} \tag{3.7}$$

In section 3.1, it was shown that for the cubic configuration, the stiffness matrix is diagonal if frame $\{B\}$ is taken at the cube's center. In that case, the "cartesian" plant is decoupled at low frequency.

At high frequency, the behavior depends on the mass matrix (evaluated at frame B) (3.8).

$$\frac{\boldsymbol{\mathcal{X}}}{\boldsymbol{\mathcal{F}}}(j\omega) \xrightarrow[\omega \to \infty]{} -\omega^2\boldsymbol{M}^{-1} \tag{3.8}$$

To have the mass matrix diagonal, the center of mass of the mobile parts needs to coincide with the B frame and the principal axes of inertia of the body also needs to coincide with the axis of the B frame.

To verify that,

- CoM above the top platform (Figure 3.5)
- The transfer functions from F to X are computed for two specific locations of the B frames:
  - center of mass: coupled at low frequency due to non diagonal stiffness matrix (Figure 3.6a)
  - center of stiffness: coupled at high frequency due to non diagonal mass matrix (Figure 3.6b)
- In both cases, we would get similar dynamics for a non-cubic stewart platform.

Payload's CoM at the cube's center It is therefore natural to try to have the cube's center and the center of mass of the moving part coincide at the same location **li01˙simul˙fault˙vibrat˙isolat˙point**.

- CoM at the center of the cube: Figure 3.7a

This is what is physically done in [9]–[13] Shown in Figure 1.1b

The obtained dynamics is indeed well decoupled, thanks to the diagonal stiffness matrix and mass matrix as the same time.

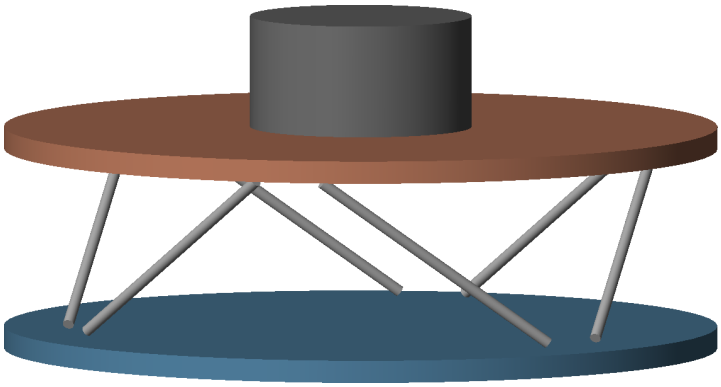

Figure 3.5: Cubic stewart platform with top cylindrical payload

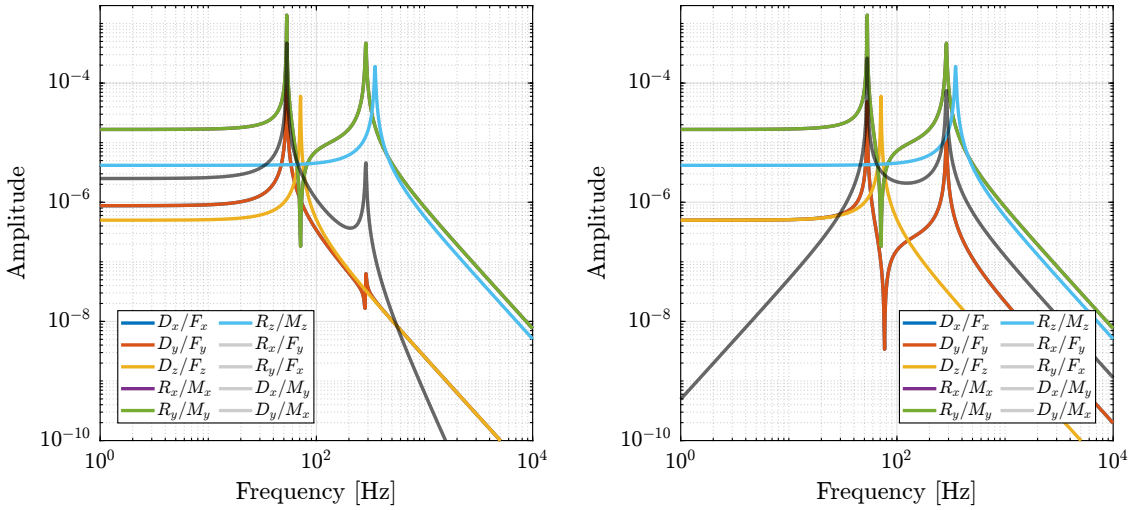

(a) $\{B\}$ at the center of mass

(b) $\{B\}$ at the cube's center

Figure 3.6: Transfer functions for a Cubic Stewart platform expressed in the Cartesian frame. Two locations of the $\{B\}$ frame are considered: at the cube's center (b) and at the center of mass of the moving body (a).

The main issue with this is that usually we want the payload to be located above the top platform, as it is the case for the nano-hexapod. Indeed, if a similar design than the one shown in Figure 3.7a was used, the x-ray beam will hit the different struts during the rotation of the spindle.

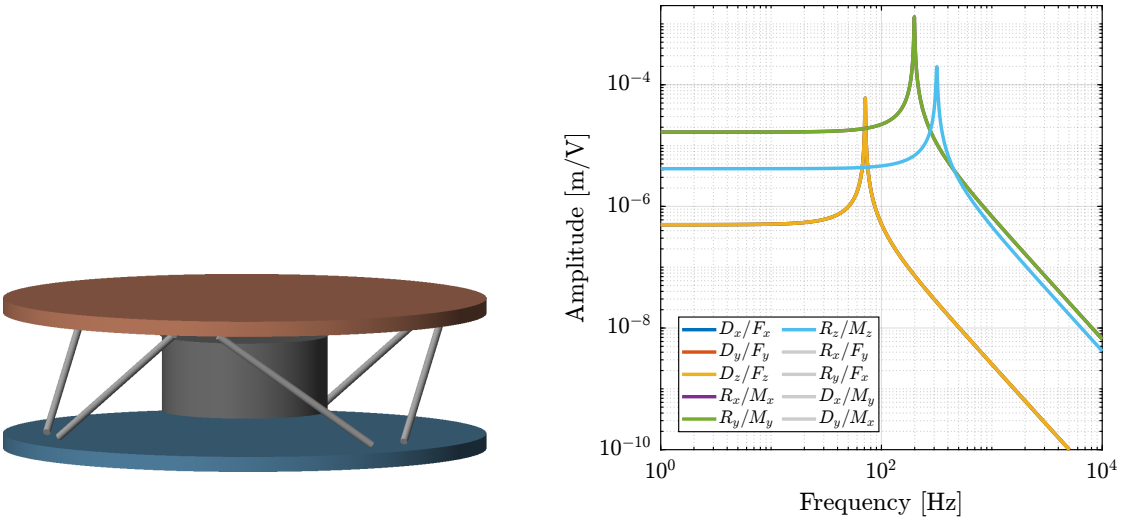

(a) Payload at the cube's center

(b) Fully decoupled cartesian plant

Figure 3.7: Cubic Stewart platform with payload at the cube's center (a). Obtained cartesian plant is fully decoupled (b)

Conclusion

- Some work to still be decoupled when considering flexible joint stiffness
  - ☐ Find the reference
- Better decoupling between the struts? Next section

Some conclusions can be drawn from the above analysis:

- Static Decoupling ¡=¿ Diagonal Stiffness matrix ¡=¿ {A} and {B} at the cube's center
- Dynamic Decoupling ¡=¿ Static Decoupling + CoM of mobile platform coincident with {A} and {B}.
- Not specific to the cubic architecture
- Same stiffness in XYZ =¿ Possible to have dynamic isotropy

3.3 Decentralized Control

From [18], the cubic configuration "*minimizes the cross-coupling amongst actuators and sensors of different legs (being orthogonal to each other)*". This would facilitate the use of decentralized control.

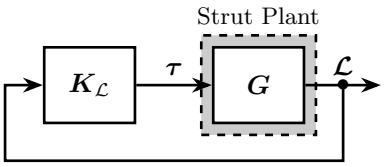

Figure 3.8: From Strut coordinate to Cartesian coordinate using the Jacobian matrix

In this section, we wish to study such properties of the cubic architecture.

Here, the plant output are sensors integrated in the Stewart platform struts. Two sensors are considered: a displacement sensor and a force sensor.

We will compare the transfer function from sensors to actuators in each strut for a cubic architecture and for a non-cubic architecture (where the struts are not orthogonal with each other).

The "strut plant" are compared for two Stewart platforms:

- with cubic architecture shown in Figure 3.5 (page 19)
- with a Stewart platform shown in Figure 3.9. It has the same payload and strut dynamics than for the cubic architecture. The struts are oriented more vertically to be far away from the cubic architecture

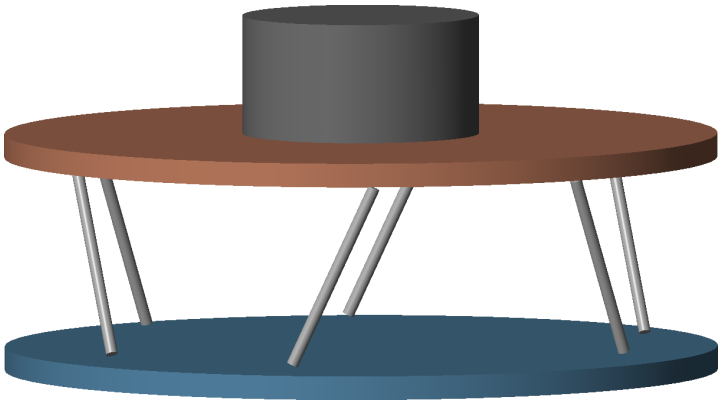

Figure 3.9: Stewart platform with non-cubic architecture

Relative Displacement Sensors The transfer functions from actuator force included in each strut to the relative motion of the struts are shown in Figure 3.10. As expected from the equations of motion from $\boldsymbol{f}$ to $\boldsymbol{\mathcal{L}}$ (2.5), the 6×6 plants are decoupled at low frequency.

At high frequency, the plant is coupled as the mass matrix projected in the frame of the struts is not diagonal.

No clear advantage can be seen for the cubic architecture (figure 3.10b) as compared to the non-cubic architecture (Figure 3.10a).

Note that the resonance frequencies are not the same in both cases as having the struts oriented more vertically changed the stiffness properties of the Stewart platform and hence the frequency of different

modes.

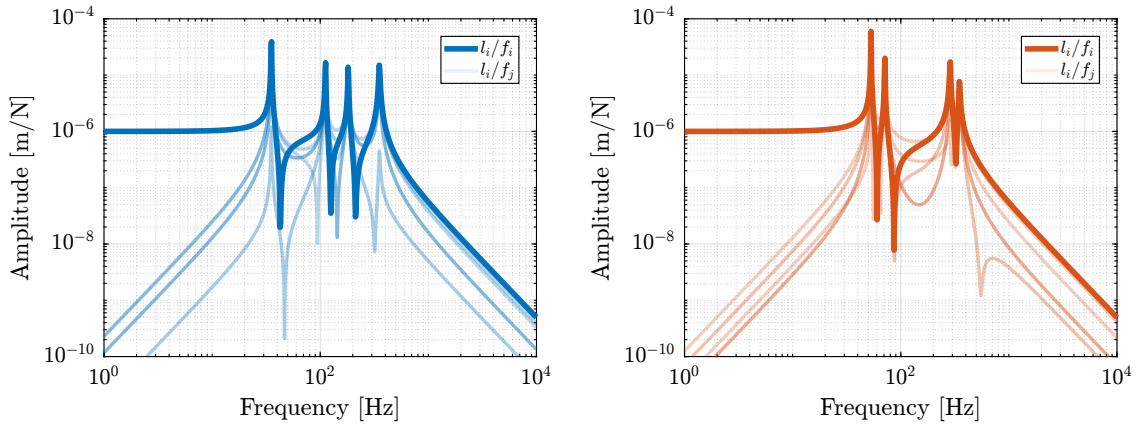

(a) Non cubic architecture **(b)** Cubic architecture

Figure 3.10: Bode plot of the transfer functions from actuator force to relative displacement sensor in each strut. Both for a non-cubic architecture (a) and for a cubic architecture (b)

Force Sensors Similarly, the transfer functions from actuator force to force sensors included in each strut are extracted both for the cubic and non-cubic Stewart platforms.

The results are shown in Figure 3.11.

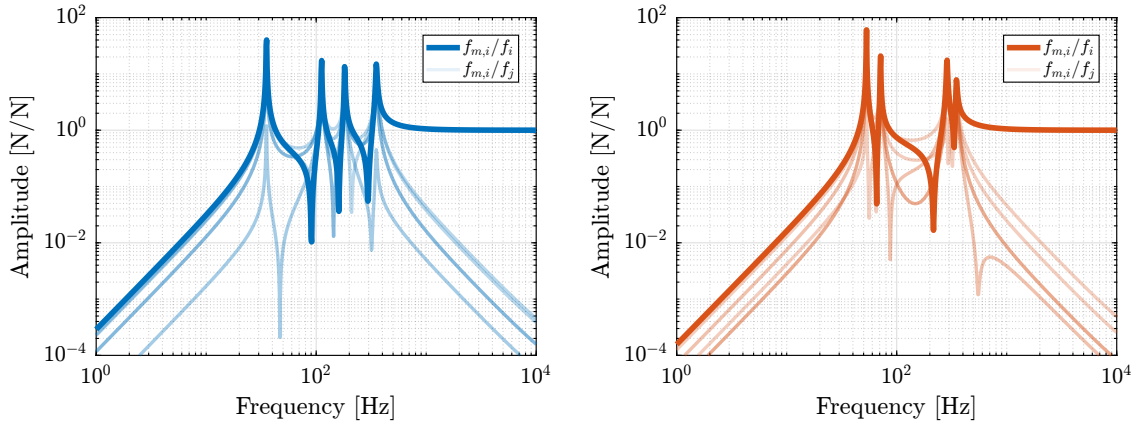

(a) Non cubic architecture **(b)** Cubic architecture

Figure 3.11: Bode plot of the transfer functions from actuator force to force sensor in each strut. Both for a non-cubic architecture (a) and for a cubic architecture (b)

Conclusion The Cubic architecture seems to not have any significant effect on the coupling between actuator and sensors of each strut and thus provides no advantages for decentralized control.

3.4 Cubic architecture with Cube's center above the top platform

As was shown in Section 3.2, the cubic architecture can have very interesting dynamical properties when the center of mass of the moving body is at the cube's center.

This is because, both the mass and stiffness matrices are diagonal. As shown in in section 3.1, the stiffness matrix is diagonal when the considered B frame is located at the cube's center.

Or, typically the $\{B\}$ frame is taken above the top platform where forces are applied and where displacements are expressed.

In this section, modifications of the Cubic architectures are proposed in order to be able to have the payload above the top platform while still benefiting from interesting dynamical properties of the cubic architecture.

There are three key parameters:

- H height of the Stewart platform (distance from fix base to mobile platform)
- H_c height of the cube, as shown in Figure 3.2a
- H_{CoM} height of the center of mass with respect to the mobile platform. It is also the cube's center.

The obtained design depends on the considered size of the cube H_c with respect to H and H_{CoM}.

Small cube When the considered cube size is smaller than twice the height of the CoM, the obtained design looks like Figure 3.12.

$$H_c < 2H_{CoM} \tag{3.9}$$

This is similar to [20], even though it is not mentioned that the system has a cubic configuration. Adjacent struts are parallel to each other, which is quite different from the typical architecture in which parallel struts are opposite to each other.

Medium sized cube Increasing the cube size with an height close to the stewart platform height leads to an architecture in which the struts are crossing.

$$2H_{CoM} < H_c < 2(H_{CoM} + H) \tag{3.10}$$

This is similar to [32] (Figure 1.2c in page 6), even though it is not cubic (but the struts are crossing).

Large cube When the cube's height is more than twice the platform height added to the CoM height, the architecture shown in Figure 3.14 is obtained.

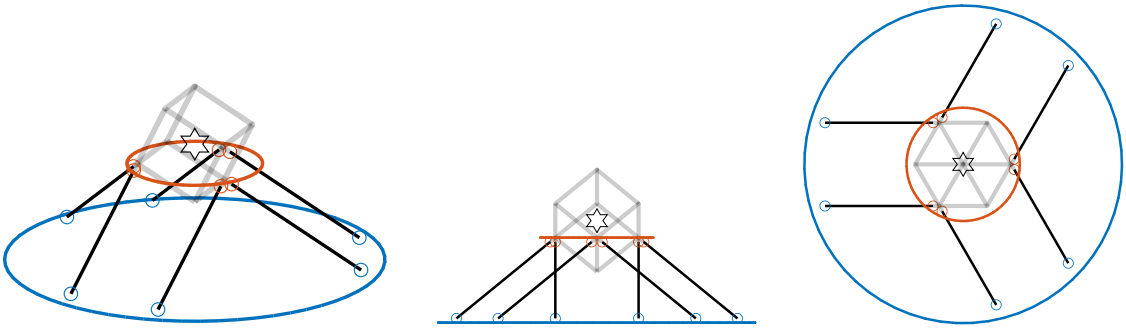

(a) Isometric view **(b)** Side view **(c)** Top view

Figure 3.12: Cubic architecture with cube's center above the top platform. A cube height of 40mm is used.

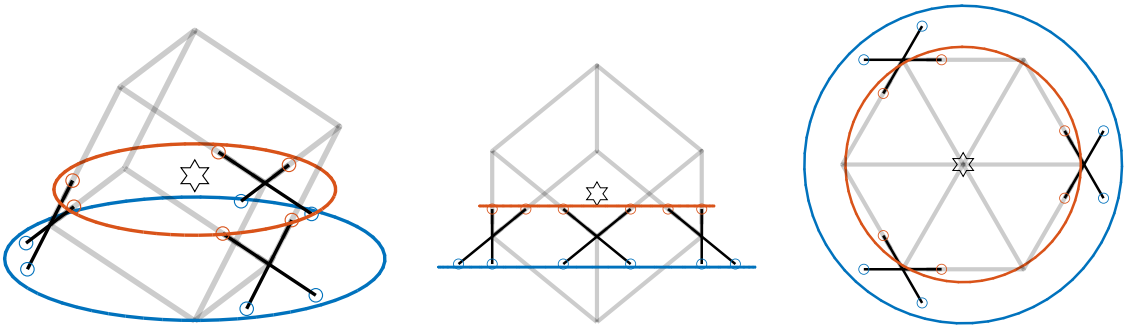

(a) Isometric view **(b)** Side view **(c)** Top view

Figure 3.13: Cubic architecture with cube's center above the top platform. A cube height of 140mm is used.

$$2(H_{CoM} + H) < H_c \tag{3.11}$$

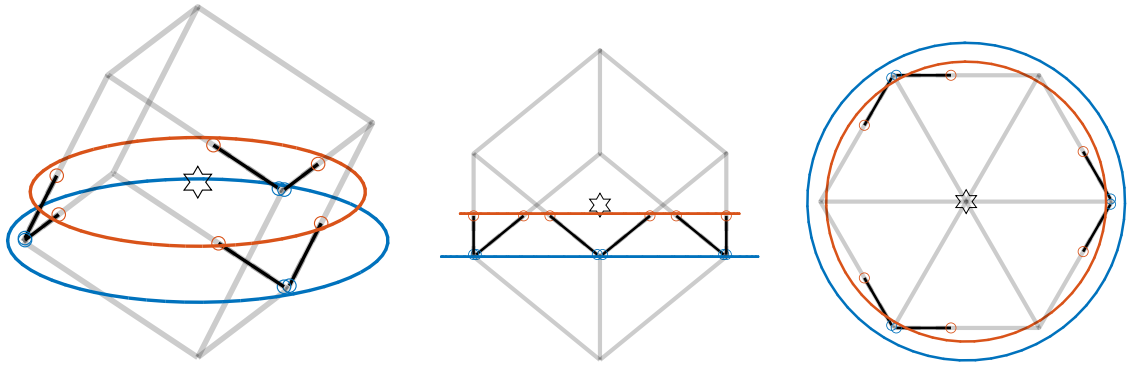

(a) Isometric view **(b)** Side view **(c)** Top view

Figure 3.14: Cubic architecture with cube's center above the top platform. A cube height of 240mm is used.

Platform size The top joints $\boldsymbol{b}_i$ are located on a circle with radius R_{b_i} (3.12a). The bottom joints $\boldsymbol{a}_i$ are located on a circle with radius R_{a_i} (3.12b).

$$R_{b_i} = \sqrt{\frac{3}{2}H_c^2 + 2H_{CoM}^2} \tag{3.12a}$$

$$R_{a_i} = \sqrt{\frac{3}{2}H_c^2 + 2(H_{CoM} + H)^2} \tag{3.12b}$$

The size of the platforms increase with the cube's size and the height of the location of the center of mass (also coincident with the cube's center). The size of the bottom platform also increases with the height of the Stewart platform.

As the rotational stiffness for the cubic architecture is scaled as the square of the cube's height (3.3), the cube's size can be determined from the requirements in terms of rotational stiffness. Then, using (3.12), the size of the top and bottom platforms can be determined.

Conclusion For each of the configuration, the Stiffness matrix is diagonal with $k_x = k_y = k_y = 2k$ with k is the stiffness of each strut. However, the rotational stiffnesses are increasing with the cube's size but the required size of the platform is also increasing, so there is a trade-off here.

We found that we can have a diagonal stiffness matrix using the cubic architecture when $\{A\}$ and $\{B\}$ are located above the top platform. Depending on the cube's size, we obtain 3 different configurations.

Conclusion

Cubic architecture can be interesting when specific payloads are being used. In that case, the center of mass of the payload should be placed at the center of the cube. For the classical architecture, it is often not possible.

Architectures with the center of the cube about the top platform are proposed to overcome this issue.

Cubic architecture are attributed a number of properties that were found to be incorrect:

- Uniform mobility
- Easy for decentralized control

4 Nano Hexapod

For the NASS, the chosen frame $\{A\}$ and $\{B\}$ coincide with the sample's point of interest, which is $150\,mm$ above the top platform.

Requirements:

- The nano-hexapod should fit within a cylinder with radius of $120\,mm$ and with a height of $95\,mm$.
- In terms of mobility: uniform mobility in XYZ directions (100um)
- In terms of stiffness: ?? Having the resonance frequencies well above the maximum rotational velocity of $2\pi\,\text{rad/s}$ to limit the gyroscopic effects. Having the resonance below the problematic modes of the micro-station to decouple from the micro-station complex dynamics.
- In terms of dynamics:
  - be able to apply IFF in a decentralized way with good robustness and performances (good damping of modes)
  - good decoupling for the HAC

The main difficulty for the design optimization of the nano-hexapod, is that the payloads will have various inertia, with masses ranging from 1 to 50kg. It is therefore not possible to have one geometry that gives good dynamical properties for all the payloads.

It could have been an option to have a cubic architecture as proposed in section 3.4, but having the cube's center 150mm above the top platform would have lead to platforms well exceeding the maximum available size. In that case, each payload would have to be calibrated in inertia before placing on top of the nano-hexapod, which would require a lot of work from the future users.

Considering the fact that it would not be possible to have the center of mass at the cube's center, the cubic architecture is not of great value here.

4.1 Obtained Geometry

Take both platforms at maximum size. Make reasonable choice (close to the final choice). Say that it is good enough to make all the calculations. The geometry will be slightly refined during the detailed mechanical design for several reason: easy of mount, manufacturability, ...

Obtained geometry is shown in Figure 4.1. Height between the top plates is 95mm. Joints are offset by 15mm from the plate surfaces, and are positioned along a circle with radius 120mm for the fixed joints

and 110mm for the mobile joints. The positioning angles (Figure 4.1b) are $[255, 285, 15, 45, 135, 165]$ degrees for the top joints and $[220, 320, 340, 80, 100, 200]$ degrees for the bottom joints.

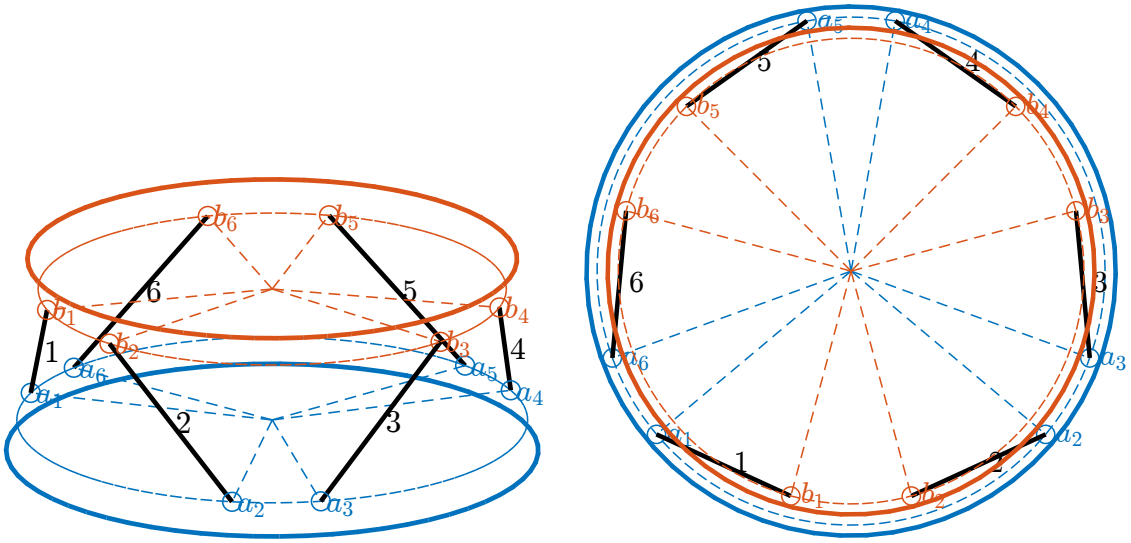

(a) Isometric view **(b)** Top view

Figure 4.1: Obtained architecture for the Nano Hexapod

This geometry will be used for:

- estimate required actuator stroke
- estimate flexible joint stroke
- when performing noise budgeting for the choice of instrumentation
- for control purposes

It is only when the complete mechanical design is finished (Section ...), that the model will be updated.

4.2 Required Actuator stroke

The actuator stroke to have the wanted mobility is computed.

Wanted mobility:

- Combined translations in the xyz directions of +/-50um (basically "cube")
- At any point of the cube, be able to do combined Rx and Ry rotations of +/-50urad
- Rz is always at 0

- Say that it is frame B with respect to frame A, but it is motion expressed at the point of interest (at the focus point of the light)

First the minimum actuator stroke to have the wanted mobility is computed. With the chosen geometry, an actuator stroke of +/-94um is found.

Considering combined rotations and translations, the wanted mobility and the obtained mobility of the Nano hexapod are shown in Figure ...

It can be seen that just wanted mobility (displayed as a cube), just fits inside the obtained mobility. Here the worst case scenario is considered, meaning that whatever the angular position in Rx and Ry (in the range +/-50urad), the top platform can be positioned anywhere inside the cube.

Therefore, in Section ..., the specification for actuator stroke is +/-100um

4.3 Required Joint angular stroke

Now that the mobility of the Stewart platform is know, the corresponding flexible joint stroke can be estimated.

- conclude on the required joint angle: 1mrad? Will be used to design flexible joints.

5 Conclusion

Inertia used for experiments will be very broad =¿ difficult to optimize the dynamics Specific geometry is not found to have a huge impact on performances. Practical implementation is important.

Geometry impacts the static and dynamical characteristics of the Stewart platform. Considering the design constrains, the slight change of geometry will not significantly impact the obtained results.

Bibliography

[1] Z. Geng and L. S. Haynes, "Six-degree-of-freedom active vibration isolation using a stewart platform mechanism," *Journal of Robotic Systems*, vol. 10, no. 5, pp. 725–744, 1993 (cit. on p. 5).

[2] Z. Geng and L. Haynes, "Six degree-of-freedom active vibration control using the stewart platforms," *IEEE Transactions on Control Systems Technology*, vol. 2, no. 1, pp. 45–53, 1994 (cit. on pp. 5, 14).

[3] Z. J. Geng, G. G. Pan, L. S. Haynes, B. K. Wada, and J. A. Garba, "An intelligent control system for multiple degree-of-freedom vibration isolation," *Journal of Intelligent Material Systems and Structures*, vol. 6, no. 6, pp. 787–800, 1995 (cit. on p. 5).

[4] J. Spanos, Z. Rahman, and G. Blackwood, "A soft 6-axis active vibration isolator," in *Proceedings of 1995 American Control Conference - ACC'95*, 1995 (cit. on p. 5).

[5] Z. H. Rahman, J. T. Spanos, and R. A. Laskin, "Multiaxis vibration isolation, suppression, and steering system for space observational applications," in *Telescope Control Systems III*, May 1998 (cit. on p. 5).

[6] D. Thayer and J. Vagners, "A look at the pole/zero structure of a stewart platform using special coordinate basis," in *Proceedings of the 1998 American Control Conference. ACC (IEEE Cat. No.98CH36207)*, 1998 (cit. on p. 5).

[7] D. Thayer, M. Campbell, J. Vagners, and A. von Flotow, "Six-axis vibration isolation system using soft actuators and multiple sensors," *Journal of Spacecraft and Rockets*, vol. 39, no. 2, pp. 206–212, 2002 (cit. on pp. 5, 14).

[8] G. Hauge and M. Campbell, "Sensors and control of a space-based six-axis vibration isolation system," *Journal of Sound and Vibration*, vol. 269, no. 3-5, pp. 913–931, 2004 (cit. on p. 5).

[9] J. McInroy, "Dynamic modeling of flexure jointed hexapods for control purposes," in *Proceedings of the 1999 IEEE International Conference on Control Applications (Cat. No.99CH36328)*, 1999 (cit. on pp. 5, 18).

[10] J. McInroy, J. O'Brien, and G. Neat, "Precise, fault-tolerant pointing using a stewart platform," *IEEE/ASME Transactions on Mechatronics*, vol. 4, no. 1, pp. 91–95, 1999 (cit. on pp. 5, 18).

[11] J. McInroy and J. Hamann, "Design and control of flexure jointed hexapods," *IEEE Transactions on Robotics and Automation*, vol. 16, no. 4, pp. 372–381, 2000 (cit. on pp. 5, 11, 17, 18).

[12] X. Li, J. C. Hamann, and J. E. McInroy, "Simultaneous vibration isolation and pointing control of flexure jointed hexapods," in *Smart Structures and Materials 2001: Smart Structures and Integrated Systems*, Aug. 2001 (cit. on pp. 5, 18).

[13] F. Jafari and J. McInroy, "Orthogonal gough-stewart platforms for micromanipulation," *IEEE Transactions on Robotics and Automation*, vol. 19, no. 4, pp. 595–603, Aug. 2003 (cit. on pp. 5, 14, 18).

[14] A. Defendini, L. Vaillon, F. Trouve, *et al.*, "Technology predevelopment for active control of vibration and very high accuracy pointing systems," in *Spacecraft Guidance, Navigation and Control Systems*, vol. 425, 2000, p. 385 (cit. on p. 5).

[15] A. Abu Hanieh, M. Horodinca, and A. Preumont, "Stiff and soft stewart platforms for active damping and active isolation of vibrations," in *Actuator 2002, 8th International Conference on New Actuators*, 2002 (cit. on p. 5).

[16] H.-J. Chen, R. Bishop, and B. Agrawal, "Payload pointing and active vibration isolation using hexapod platforms," in *44th AIAA/ASME/ASCE/AHS/ASC Structures, Structural Dynamics, and Materials Conference*, Apr. 2003 (cit. on p. 5).

[17] A. A. Hanieh, "Active isolation and damping of vibrations via stewart platform," Ph.D. dissertation, Université Libre de Bruxelles, Brussels, Belgium, 2003 (cit. on pp. 5, 14).

[18] A. Preumont, M. Horodinca, I. Romanescu, *et al.*, "A six-axis single-stage active vibration isolator based on stewart platform," *Journal of Sound and Vibration*, vol. 300, no. 3-5, pp. 644–661, 2007 (cit. on pp. 5, 14, 20).

[19] B. N. Agrawal and H.-J. Chen, "Algorithms for active vibration isolation on spacecraft using a stewart platform," *Smart Materials and Structures*, vol. 13, no. 4, pp. 873–880, 2004 (cit. on p. 5).

[20] K. Furutani, M. Suzuki, and R. Kudoh, "Nanometre-cutting machine using a stewart-platform parallel mechanism," *Measurement Science and Technology*, vol. 15, no. 2, pp. 467–474, 2004 (cit. on pp. 5, 23).

[21] Y. Ting, H.-C. Jar, and C.-C. Li, "Design of a 6dof stewart-type nanoscale platform," in *2006 Sixth IEEE Conference on Nanotechnology*, 2006 (cit. on p. 5).

[22] Y. Ting, C.-C. Li, and T. V. Nguyen, "Composite controller design for a 6dof stewart nanoscale platform," *Precision Engineering*, vol. 37, no. 3, pp. 671–683, 2013 (cit. on p. 5).

[23] Y. Ting, H.-C. Jar, and C.-C. Li, "Measurement and calibration for stewart micromanipulation system," *Precision Engineering*, vol. 31, no. 3, pp. 226–233, 2007 (cit. on p. 5).

[24] Z. Zhang, J. Liu, J. Mao, Y. Guo, and Y. Ma, "Six dof active vibration control using stewart platform with non-cubic configuration," in *2011 6th IEEE Conference on Industrial Electronics and Applications*, Jun. 2011 (cit. on p. 5).

[25] Z. Du, R. Shi, and W. Dong, "A piezo-actuated high-precision flexible parallel pointing mechanism: Conceptual design, development, and experiments," *IEEE Transactions on Robotics*, vol. 30, no. 1, pp. 131–137, 2014 (cit. on p. 5).

[26] W. Chi, D. Cao, D. Wang, *et al.*, "Design and experimental study of a vcm-based stewart parallel mechanism used for active vibration isolation," *Energies*, vol. 8, no. 8, pp. 8001–8019, 2015 (cit. on p. 5).

[27] J. Tang, D. Cao, and T. Yu, "Decentralized vibration control of a voice coil motor-based stewart parallel mechanism: Simulation and experiments," *Proceedings of the Institution of Mechanical Engineers, Part C: Journal of Mechanical Engineering Science*, vol. 233, no. 1, pp. 132–145, 2018 (cit. on p. 5).

[28] J. Jiao, Y. Wu, K. Yu, and R. Zhao, "Dynamic modeling and experimental analyses of stewart platform with flexible hinges," *Journal of Vibration and Control*, vol. 25, no. 1, pp. 151–171, 2018 (cit. on p. 5).

[29] C. Wang, X. Xie, Y. Chen, and Z. Zhang, "Investigation on active vibration isolation of a stewart platform with piezoelectric actuators," *Journal of Sound and Vibration*, vol. 383, pp. 1–19, Nov. 2016 (cit. on p. 5).

[30] M. Beijen, M. Heertjes, J. V. Dijk, and W. Hakvoort, "Self-tuning mimo disturbance feedforward control for active hard-mounted vibration isolators," *Control Engineering Practice*, vol. 72, pp. 90–103, 2018 (cit. on p. 5).

[31] D. Tjepkema, "Active hard mount vibration isolation for precision equipment [ph. d. thesis]," Ph.D. dissertation, 2012 (cit. on p. 5).

[32] X. Yang, H. Wu, B. Chen, S. Kang, and S. Cheng, "Dynamic modeling and decoupled control of a flexible stewart platform for vibration isolation," *Journal of Sound and Vibration*, vol. 439, pp. 398–412, Jan. 2019 (cit. on pp. 5, 23).

[33] M. Naves, "Design and optimization of large stroke flexure mechanisms," Ph.D. dissertation, Univeristy of Twente, 2020 (cit. on p. 5).

[34] M. Naves, W. Hakvoort, M. Nijenhuis, and D. Brouwer, "T-flex: A large range of motion fully flexure-based 6-dof hexapod," in *20th EUSPEN International Conference & Exhibition, EUSPEN 2020*, EUSPEN, 2020, pp. 205–208 (cit. on p. 5).